data for concentration polarization at each measurement potential was performed according to conventional procedures, and this correction was incorporated into the *J-E* data of Fig. 2B. No correction was made for double-layer effects on the rate constant, although the ions being reduced were dipositively charged. This correction is extremely small for a semiconductor-liquid interface because at the electrolyte concentration we used, the differential capacitance of the semiconductor is about one-thousandth that of the Helmholtz layer (compare with Fig. 1). The Frumkin correction that relates the bulk and surface concentrations of a redox-active ion in the solution is negligible under such experimental conditions (W. J. Royea, O. Krüger, N. S. Lewis, in preparation).

18. Further variation in driving force was precluded at negative potentials, because of the formation of nonrectifying junctions, and in the positive region, because of the change in the rate-limiting step to bulk recombination-diffusion [M. L. Rosenbluth and N. S. Lewis, *J. Am. Chem. Soc.* **108**, 4689 (1986)]. The rate constants determined here primarily reflect the conduction-band kinetic process because the valence band process of Si-CH_3OH–dimethylferrocene$^{+/0}$ contacts, which was identified as bulk recombination-diffusion in this small band-gap semiconductor, exhibits a different dependence of *J* on [A]. In addition, the use of ohmic-selective contacts has shown directly that the *J* in the systems described here is associated with electron transfer from the conduction band as opposed to hole transfer into the valence band [M. X. Tan, C. N. Kenyon, N. S. Lewis, *J. Phys. Chem.* **98**, 4959 (1994)].
19. Morrison has reported rate constant values of 10^{-20} to 10^{-15} cm^4 s^{-1} for electron transfer from ZnO to various acceptors in aqueous solution [S. R. Morrison, *Surf. Sci.* **15**, 363 (1969); ——— and T. Freund, *ibid.* **9**, 119 (1968)]. A $k_{et,max}$ of 10^{-16} cm^4 s^{-1} was suggested by the trend of the observed capture cross section versus standard reduction potential, although the variation of λ by >1 eV for the series of acceptors used precludes a quantitative evaluation of the generality of this observation. In addition, the anomalously steep decline in rate constant observed at high exoergicity, along with an anomalous pH dependence of the rate constant for reduction of aqueous $Fe(CN)_6^{3-}$, led these authors to suggest a strong role for inner-sphere electron transfer, adsorption processes, or both in these kinetic events. Our rate constant data are in qualitative agreement with the value of $k_{et,max}$ suggested by these authors, although such agreement might well be fortuitous.
20. Y. Rosenwaks, B. R. Thacker, R. K. Ahrenkiel, A. J. Nozik, *J. Phys. Chem.* **96**, 10096 (1992).
21. S. Dai, thesis, University of Tennessee, Knoxville (1990); F. Williams, *U.S. Dep. Energy Rep. 91015008* (1991).
22. R. A. Marcus, *J. Chem. Phys.* **43**, 679 (1965).
23. B. B. Smith and C. A. Koval, *J. Electroanal. Chem.* **277**, 43 (1990).
24. Supported by NSF grant CHE-9634152.

25 June 1996; accepted 13 September 1996

Maturation of a Central Glutamatergic Synapse

G.-Y. Wu, R. Malinow, H. T. Cline*

Whole-cell recordings from optic tectal neurons in *Xenopus* tadpoles were used to study the maturation of a glutamatergic synapse. The first glutamatergic transmission is mediated only by *N*-methyl-D-aspartate (NMDA) receptors and is silent at resting potentials. More mature synapses acquire transmission by α-amino-3-hydroxy-5-methyl-4-isoxazole propionic acid (AMPA) receptors. This maturational program is mimicked by postsynaptic expression of constitutively active calcium-calmodulin–dependent protein kinase II (CaMKII). Newly formed synapses may be silent unless sufficient depolarization is provided by coincident activity that could activate postsynaptic CaMKII, resulting in the appearance of AMPA responses.

Most excitatory synapses in the vertebrate central nervous system use glutamate to mediate synaptic transmission (*1*) through two types of ionotropic receptors, the AMPA and NMDA receptors. AMPA and NMDA receptors are distinguishable by their pharmacological and biophysical properties (*2*). In particular, at hyperpolarized potentials, NMDA receptor channels are to a large extent blocked by Mg^{2+}, whereas AMPA receptors are capable of transmission. Although a single neuron may express both receptors (*3*), their distribution at individual synapses is less clear (*4*, *5*). Recent studies have suggested that many synapses in early postnatal hippocampus have only functional NMDA receptors (*6*–*9*). A wide spectrum of developmental stages can be studied in a single tadpole optic tectum because neurons are in different developmental stages along the rostrocaudal (RC) axis (*10*). We investigated the physiological properties of early synaptic development in this system and examined whether retinotectal synapses initially transmit with only NMDA receptors and add an AMPA component with maturation.

We also investigated the role of the calcium-calmodulin–dependent protein kinase II (CaMKII) in synaptic maturation. The expression of this enzyme is developmentally regulated (*11*), is concentrated in synaptic regions (*12*, *13*), and has been implicated in control of neuronal growth and synaptogenesis (*14*–*16*), as well as in activity-dependent synaptic plasticity (*17*–*21*). To determine whether CaMKII activity is sufficient to cause maturation of glutamatergic synapses, we increased CaMKII activity specifically in postsynaptic tectal neurons, and not in the presynaptic retinal afferents, by infecting tectal cells with a vaccinia virus (*22*) carrying the gene for a truncated calcium-calmodulin–independent form of CaMKII (tCaMKII) (*20*).

Morphological development of tectal neurons correlates well with position of the cell body along the RC axis (Fig. 1B), indicating that position along the RC axis can be used to select neurons at different stages of maturation. Whole-cell recordings were obtained from tectal neurons at different sites along the RC axis, and synaptic transmission was evoked by a stimulating electrode placed in the optic chiasm (Fig.

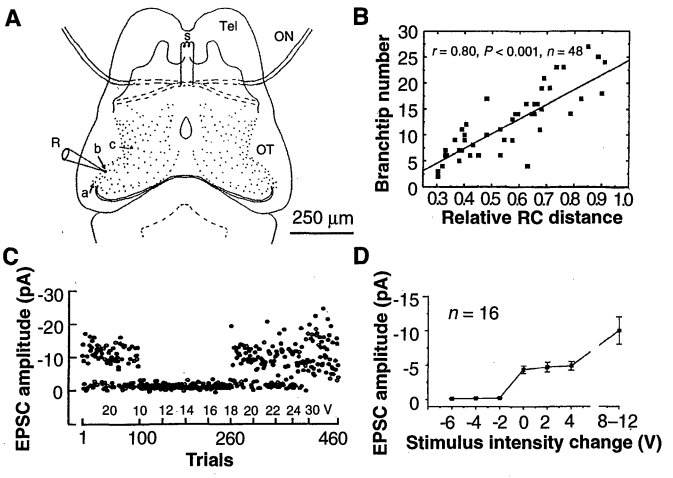

Fig. 1. (**A**) Diagram of the whole-brain preparation showing the stimulating electrode (S) in the optic chiasm and the recording patch-pipette (R) in the optic tectal cell body region (OT). Tel, telencephalon; ON, optic nerve. (**B**) Plot of dendritic branchtip number versus relative distance from the caudal border of the optic tectum. (**C**) EPSC amplitude does not change over a range of stimulus intensities above threshold, indicating single-fiber excitation. Plot of EPSC amplitude versus trials. Stimulus intensity was changed where indicated. (**D**) Ensemble average from 16 cells. The stimulus duration was varied (30 to 150 μs) so that threshold responses were obtained at about 20-V stimulus, indicated as 0 V on the *x* axis. After the threshold was set, voltage setting was changed (*x* axis) to determine response sensitivity to variations in stimulus intensity.

Cold Spring Harbor Laboratory, Cold Spring Harbor, NY 11724, USA.

*To whom correspondence should be addressed. E-mail: cline@cshl.org

1A) (23). The stimulus intensity was set to elicit a stable minimal synaptic response. As stimulus intensity was increased, responses appeared at a threshold stimulus and did not increase in amplitude over a relatively wide range of stimulus intensities (Fig. 1, C and D). This result indicates that the minimal synaptic responses we elicited represent transmission from a single retinal axon onto the monitored postsynaptic tectal cell (24, 25); however, each retinal axon may make multiple synaptic contacts with a single tectal cell.

We examined retinotectal excitatory transmission onto more mature cells by recording from neurons in the rostral third of tectum (Fig. 2A). Responses displayed a rapid AMPA receptor–mediated component and a slower, voltage-dependent NMDA receptor–mediated component. Recordings from younger neurons in caudal tectum showed responses mediated primarily by NMDA receptors (Fig. 2B). In some cells, all synaptic responses were mediated by NMDA receptors (for example, Fig. 4A) and could be blocked by D, L-2-amino-5-phosphonovaleric acid (APV) (26). The AMPA/NMDA ratio of evoked responses increased along the RC axis of the tectum (Fig. 2C) (27). Single-fiber excitation indicated that this increase is caused by enhanced AMPA transmission with no change in NMDA transmission (Fig. 2D).

Spontaneous miniature EPSCs (mEPSCs) (28) were recorded at depolarized and hyperpolarized potentials to evaluate events at single synapses (29). Individual synapses in mature tectal neurons in rostral tectum showed both AMPA and NMDA components (Fig. 3Ab) (4). In contrast, immature neurons showed pure NMDA spontaneous currents (Fig. 3Aa). Events recorded at depolarized potentials were not analyzed quantitatively because of the inability to distinguish reliably the beginning and end of events with only a slow component. The frequency and amplitude of AMPA mEPSCs, recorded at −60 mV, increased significantly as a function of cell body position along the RC axis (Fig. 3, B and C). The increased frequency of events at hyperpolarized potentials has traditionally been interpreted as an increase in presynaptic function (5, 28), although the appearance of AMPA receptor sensitivity at existing synapses with only NMDA receptor function could also explain this observation (6–8).

To distinguish between a change in presynaptic function and the addition of AMPA responses to preexisting NMDA synapses, we analyzed the failure rate of evoked responses at depolarized and hyperpolarized potentials (30). If the developmental increase in mEPSC frequency were due to a generalized increase in presynaptic function, then one should observe a decrease in synaptic failure rate at both hyperpolarized and depolarized potentials as neurons mature. Comparison of single-fiber responses across the RC axis showed a decrease in synaptic failure rate at hyperpolarized potentials but no change in failure rate at depolarized potentials (Fig. 4). This result argues against a generalized increase in presynaptic function during this developmental period.

Synapses with only NMDA receptor function can be detected by comparing synaptic failure rates recorded at hyperpolarized and depolarized potentials (7). In general, more failures were recorded at hyperpolarized than at depolarized potentials (Fig. 4H), indicating that a significant fraction of synaptic events is mediated solely by action on NMDA receptors (mean ± SEM, 47 ± 5%; n = 41). The fraction of respons-

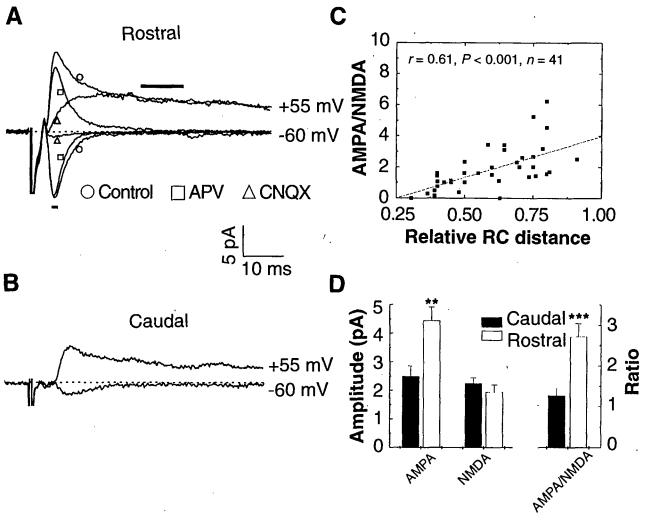

Fig. 2. Increase in the AMPA component of the synaptic response with neuronal development. (**A**) Retinotectal-evoked synaptic responses recorded in rostral optic tectum have mixed AMPA and NMDA components. Upper three traces obtained at +55 mV, lower three traces obtained at −60 mV. Symbols indicate drugs (Control, no drugs; APV, 100 μM DL-APV; CNQX, 10 μM) in perfusate during recording. Horizontal black bars show positions of windows for measuring amplitudes of NMDA and AMPA currents. (**B**) Evoked synaptic transmission recorded from a neuron in caudal optic tectum. Traces in (A) and (B) are averages of 10 to 50 consecutive responses. (**C**) AMPA/NMDA ratio of single-fiber responses for neurons recorded at various positions along the RC axis. (**D**) Average amplitudes (mean ± SEM) of AMPA and NMDA responses and their ratio for the pooled population of rostral (RC position 0.62 to 1.0; n = 20) and caudal (RC positions 0.25 to RC 0.62; n = 21) neurons. AMPA responses in rostral neurons, 4.4 ± 0.4 pA; caudal neurons, 2.4 ± 0.4 pA. NMDA responses in rostral neurons, 1.9 ± 0.3 pA; caudal neurons, 2.2 ± 0.2 pA. Average AMPA/NMDA ratio in rostral neurons, 2.7 ± 0.3; caudal neurons, 1.3 ± 0.2. $^{**}P < 0.01$, $^{***}P < 0.001$.

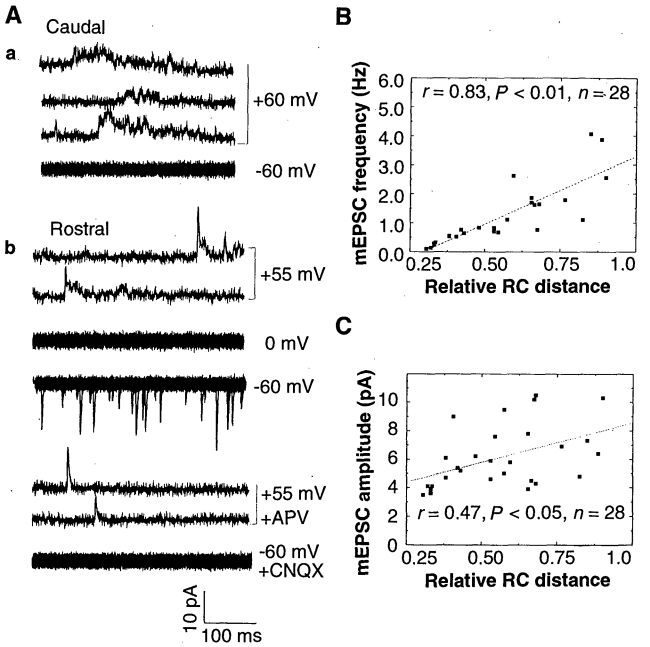

Fig. 3. Developmental increase in AMPA responses at single synapses revealed by spontaneous miniature synaptic events. (**A**) mEPSCs recorded from neurons in caudal tectum (a) and rostral tectum (b), under different recording conditions as indicated (n = 28). (a) In recordings from immature neuron, pure NMDA receptor–mediated mEPSCs can be recorded as indicated by the presence of spontaneous events in individual traces at +60 mV but not at −60 mV. (b) In mature neurons, individual traces show that mEPSCs recorded at +55 mV have fast and slow components; the latter are blocked by hyperpolarization or APV. The mEPSCs recorded at −60 mV are completely blocked by CNQX. Superimposed traces recorded at 0 mV show no synaptic responses. Each superimposed recording is composed of 20 consecutive traces. An increase in frequency (**B**) and amplitude (**C**) of AMPA mEPSC, recorded at −60 mV in the presence of Mg^{2+}, as a function of distance along the RC axis.

es onto a cell mediated purely by NMDA receptors decreases with neuronal maturity (Fig. 4G). These data support the interpretation that immature synapses initially transmit only with NMDA receptors and that as synapses mature, they acquire AMPA receptor function. This interpretation can explain the selective increase in the amplitude of evoked AMPA receptor transmission, the increased frequency of spontaneous AMPA receptor mEPSCs, as well as the decrease in failures at hyperpolarized potentials with no change in failures at depolarized potentials.

Although the amplitude of evoked NMDA responses showed no change along the RC axis, the decay time (peak to 50% amplitude) of NMDA responses was significantly ($P < 0.001$) shorter in more mature rostral neurons (mean ± SEM, 88 ± 7 ms; n =15) than in caudal neurons (mean ± SEM, 187 ± 15 ms; n = 18) as seen in rat cortical neurons (*31*, *32*). We observed no difference in the voltage dependence of NMDA responses between rostral or caudal neurons (*26*).

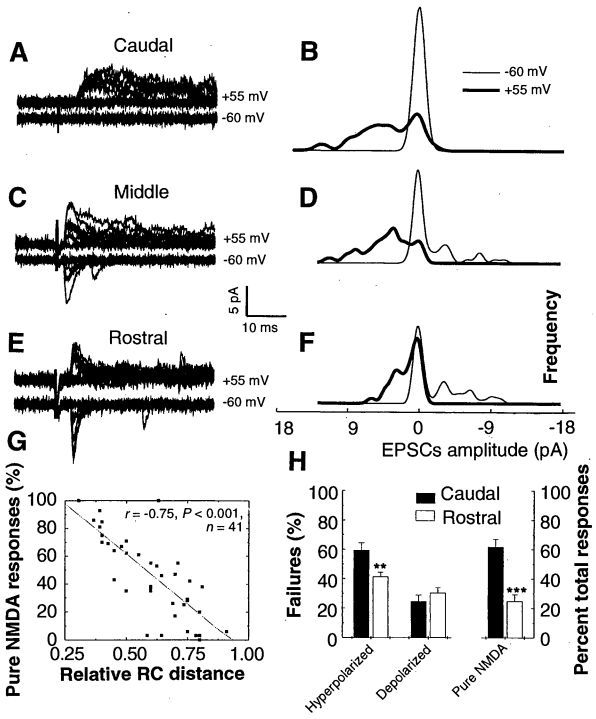

Fig. 4. Decrease in the fraction of pure NMDA responses with neuronal development. (**A**, **C**, **E**) Evoked synaptic currents recorded at +55 mV and −60 mV from neurons located in caudal (A), middle (C), and rostral (E) optic tectum. (**B**, **D**, **F**) Amplitude distribution histograms of synaptic currents recorded at −60 mV (light line) and +55 mV (dark line) are shown to the right of each set of recordings (*30*). The peaks at 0 amplitude represent synaptic failures. Failure rates at the two potentials are similar in the neuron from rostral tectum, but are successively more disparate in neurons from middle and caudal tectum. (**G**) The fraction of total events that are mediated purely by NMDA receptors decreases from about 100% in caudal neurons to about 5% in rostral neurons. (**H**) Failure rates at hyperpolarized potentials decrease significantly from 59 ± 5% in caudal tectum to 41 ± 3% in rostral tectum. Failure rates at depolarized potentials increase from 24 ± 4% in caudal tectum to 30 ± 3% in rostral tectum. The fraction of pure NMDA responses decreases from 62 ± 5% in caudal neurons to 25 ± 4% in rostral neurons (mean ± SEM, $^{**}P < 0.01$, $^{***}P < 0.001$).

To determine whether increasing CaMKII activity in the postsynaptic tectal neurons promotes the maturation of retinotectal glutamatergic synapses, we infected tectal neurons with a recombinant vaccinia virus carrying genes for the truncated constitutively active CaMKII (tCaMKII) plus the reporter, β-galactosidase (β-Gal) (*14*, *20*). Control studies were done with a virus carrying only the gene for β-Gal. Most cells in the brain are infected and express β-Gal within 36 hours after injection of virus into the brain ventricle (*22*). Retinal ganglion cells, which are the afferents activated by the stimulating electrode, do not express foreign protein (*22*). We recorded evoked and spontaneous synaptic responses from tectal neurons 3 days after injection of the tCaMKII virus (*33*), when calcium-calmodulin–independent CaMKII activity in the brain is increased by 50% over the control value (*14*). Neurons were recorded from the caudal half of differentiated tectum, where physiological measures of synaptic transmission in control animals show an immature phenotype. As in hippocampal neurons (*20*), expression of tCaMKII did not affect the passive membrane properties of postsynaptic cells (*26*).

Expression of tCaMKII in postsynaptic cells mimicked every measure of synaptic maturation analyzed related to AMPA receptor function. Single-fiber responses in tCaMKII-infected neurons showed a significantly larger AMPA component than uninfected or β-Gal–infected controls, with no change in the NMDA component of evoked transmission (Fig. 5C). The AMPA response in tCaMKII-infected neurons was blocked by CNQX (*26*). The AMPA/NMDA ratio in tCaMKII-infected neurons was significantly greater ($P < 0.001$) than in control neurons (Fig. 5C).

Neurons infected with the tCaMKII virus had significantly fewer failures at hyperpolarized potentials, with no significant change in failures at depolarized potentials compared with uninfected or β-Gal–infected neurons (Fig. 5, A and B). A smaller fraction of transmission was mediated by pure NMDA responses in tCaMKII-infected cells than in either uninfected or β-Gal–infected neurons in caudal tectum. The fraction of pure NMDA transmission in the tCaMKII neurons (Fig. 5D) was comparable

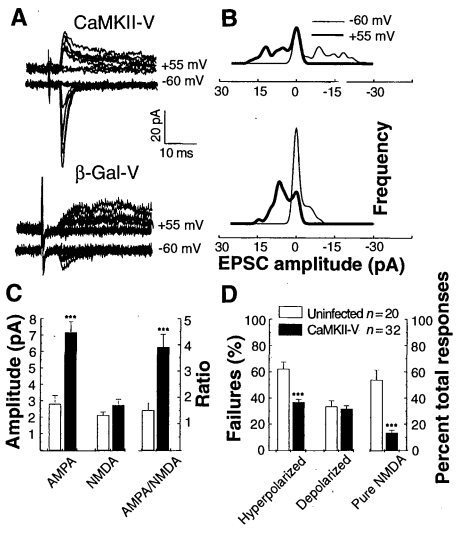

Fig. 5. Selective increase in the AMPA component of evoked synaptic responses by CaMKII. (**A**) Sequence of 10 consecutive, individual evoked responses obtained at the indicated holding potential from neurons infected with tCaMKII-V (top) or β-Gal-V (bottom). (**B**) Amplitude distribution histograms of the responses at +55 mV (dark lines) and −60 mV (light lines) generated from the recordings in (A). (**C**) Graph of the average amplitudes of AMPA and NMDA synaptic components and their ratio in uninfected or tCaMKII-infected neurons. Amplitude of AMPA responses: uninfected controls, 2.8 ± 0.5 pA, n = 20; β-Gal, 3.0 ± 0.7 pA, n = 11; tCaMKII, 7.1 ± 0.6 pA, n = 32; NMDA responses: uninfected controls, 2.1 ± 0.2 pA, n = 20; β-Gal, 2.7 ± 0.2 pA, n = 11; tCaMKII, 2.7 ± 0.4 pA, n = 32; AMPA/NMDA ratio: 1.5 ± 0.3; β-Gal, 1.30 ± 0.4; tCaMKII, 3.9 ± 0.5; mean ± SEM, $^{***}P < 0.001$. (**D**) Graph of failure rate at hyperpolarized and depolarized potentials and the calculated fraction of transmission mediated by pure NMDA responses in uninfected or tCaMKII-infected neurons. Hyperpolarized failures: uninfected controls, 62 ± 5%, n = 20; β-Gal, 55 ± 4%, n = 11; tCaMKII, 37 ± 2%, n = 32; depolarized failures: uninfected controls, 33 ± 4%, n = 20; β-Gal, 24 ± 4%, n = 11; tCaMKII, 32 ± 2%, n = 32); fraction of pure NMDA responses: uninfected controls, 54 ± 8%, n = 20; β-Gal, 60 ± 6%, n = 9; tCaMKII, 13 ± 2%, n = 32; mean ± SEM, $^{***}P <$ 0.001. No significant differences were observed between β-Gal and uninfected control neurons.

to that recorded from neurons in rostral tectum of uninfected control animals (Fig. 4H).

If tCaMKII produces an increase in the number of AMPA-sensitive synapses, then one would predict an increase in the frequency of mEPSCs recorded at hyperpolarized potentials, as was observed during synaptic maturation. The frequency of AMPA receptor–mediated mEPSCs was significantly greater ($P < 0.001$) in tCaMKII neurons than in uninfected or β-Gal–infected neurons [mEPSC frequency: 2.85 ± 0.5 Hz in tCaMKII neurons ($n = 28$), 1.32 ± 0.2 Hz in uninfected neurons ($n = 64$), 1.4 ± 0.3 Hz in β-Gal–infected neurons ($n = 32$)] and was comparable to that recorded from uninfected rostral neurons (2.05 ± 0.3 Hz). Similar to what has been observed with synaptic maturation, AMPA mEPSC amplitude in tCaMKII neurons was significantly greater ($P < 0.01$) than that in uninfected or β-Gal–infected neurons (mEPSC amplitude: 8.2 ± 0.6 pA in tCaMKII neurons, 5.7 ± 0.3 pA in uninfected neurons, 5.9 ± 0.4 pA in β-Gal–infected neurons) and was comparable to the amplitude recorded from uninfected rostral neurons (7.0 ± 0.7 pA).

Recent studies on glutamatergic transmission have focused on changes in NMDA receptor function and plasticity (*9*, *31*, *32*, *34*–*36*). For the stages of synaptic maturation examined in this study, we find marked changes in the amplitude of the AMPA receptor synaptic component, with no significant change in the amplitude of the NMDA receptor synaptic component. Our data can be explained by a model in which individual presynaptic cells make a small number of synapses onto each postsynaptic cell. The initial synaptic contacts transmit only with NMDA receptors. As neurons and synapses mature, individual contacts between these two cells acquire AMPA receptor function independently. The AMPA and NMDA composition of all contacts between individual retinal ganglion and tectal cells does not appear to change in a homogeneous manner (because there are intermediate values for the fraction of pure NMDA responses) (Fig. 4G). A general increase in presynaptic function over this maturational gradient does not appear to occur, because we observed no significant change in the amplitude or failure rate of transmission mediated by NMDA receptors (*37*).

The results with recombinant viral expression support a model in which increased postsynaptic CaMKII activity selectively enhances AMPA receptor function. In synapses that normally show only NMDA receptor sensitivity, AMPA responses appear; in synapses that show some AMPA receptor sensitivity, a greater AMPA response is obtained. A general increase in presynaptic function after increased postsynaptic CaMKII activity, which would be the classical interpretation for the observed increase in mEPSC frequency, is unlikely in our experiments because NMDA receptor–sensitive transmission appears to be unaffected.

During the developmental period analyzed, the optic tectum normally processes visual information even as new retinotectal synaptic connections are forming (*38*). One way to ensure transmission fidelity while allowing formation of randomly made trial synapses would be to make these new synapses pure NMDA and thus functionally silent at resting potentials. In this instance, new randomly made synapses will transmit information only if other, more mature synapses, are active. Furthermore, if correlated converging activity causes the addition of an AMPA component to the synapse, as suggested by studies in the hippocampus (*7*–*9*) and the present data with tCaMKII expression, then only those pure NMDA synaptic contacts that are coactive with other depolarizing inputs would go through this maturational process (*39*). Such a mechanism for controlling which synapses mature (that is, develop an AMPA component) would select for inputs that are correlated with, and thus presumably functionally relevant to, other converging inputs.

REFERENCES AND NOTES:

1. M. Hollman and S. Heinemann, *Annu. Rev. Neurosci.* **17**, 31 (1994).
2. B. Edmonds, A. J. Gibb, D. Colquhoun, *Annu. Rev. Physiol.* **57**, 495 (1995).
3. S. Hestrin *et al.*, *Cold Spring Harbor Symp. Quant. Biol.* **55**, 87 (1990).
4. J. M. Bekkers and C. F. Stevens, *Nature* **341**, 230 (1989).
5. D. M. Kullmann and S. A. Siegelbaum, *Neuron* **15**, 997 (1995).
6. D. M. Kullmann, *ibid.* **12**, 1111 (1994).
7. D. Liao, N. A. Hessler, R. Malinow, *Nature* **375**, 400 (1995).
8. J. T. R. Isaac, R. A. Nicoll, R. C. Malenka, *Neuron* **15**, 427 (1995).
9. G. M. Durand, Y. Kovalchuk, A. Konnerth, *Nature* **381**, 71 (1996).
10. G. Lazar, *J. Anat.* **116**, 347 (1973).
11. H. Schulman, *Curr. Opin. Cell Biol.* **5**, 247 (1993).
12. P. T. Kelly, T. L. McGuinness, P. Greengard, *Proc. Natl. Acad. Sci. U.S.A.* **81**, 945 (1984).
13. M. B. Kennedy, T. L. McGuinness, P. Greengard, *J. Neurosci.* **3**, 818 (1983).
14. D.-J. Zou and H. T. Cline, *Neuron* **16**, 529 (1996).
15. W. K. Scholz, C. Baitinger, H. Schulman, P. T. Kelly, *J. Neurosci.* **8**, 1039 (1988).
16. Y. Goshima, S. Ohsako, T. Yamauchi, *ibid.* **13**, 559 (1993).
17. A. P. Braun and H. Schulman, *Annu. Rev. Physiol.* **57**, 417 (1995).
18. L. C. Griffith *et al.*, *Neuron* **10**, 501 (1993).
19. J.-H. Wang and P. T. Kelly, *ibid.* **15**, 443 (1995).
20. D. L. Pettit, S. Perlman, R. Malinow, *Science* **266**, 1881 (1994).
21. S. Glazewski, C.-M. Chen, A. Silva, K. Fox, *ibid.* **272**, 421 (1996).
22. G.-Y. Wu, D.-J. Zou, T. Koothan, H. T. Cline, *Neuron* **14**, 681 (1995).
23. Stage 47 to 48 albino *Xenopus* tadpoles were anesthetized in 0.02% MS222 and their brains rapidly dissected out. The tectum was filleted along the midline and laid out in a recording chamber so that the ventricular surface faced up. RC distance was measured as the relative distance from the caudal border of the tectum, with the maximal RC distance equal to 1. Whole-cell recordings were taken from neurons at different positions along the RC axis of the tectum, selected under visual guidance. The pipette solution consisted of 80 mM cesium methanesulfate, 10 mM EGTA, 20 mM tetraethylammonium, 5 mM $MgCl_2$, 2 mM adenosine triphosphate, 0.3 mM guanosine triphosphate, and 20 mM Hepes (pH 7.2) with CsOH. The bathing solution contained 115 mM NaCl, 4 mM KCl, 3 mM $CaCl_2$, 3 mM $MgCl_2$, 5 mM Hepes, 10 μM glycine, 100 μM picrotoxin, and 10 mM glucose and was continually perfused over the brain. Neurons had input resistances in the range of 1 to 4 gigohm. Series resistance was less than 50 megohm and was monitored throughout an experiment. Synaptic transmission was elicited by passing current either through a glass stimulating electrode or a bipolar tungsten electrode placed in the optic chiasm; stimuli were delivered at 0.2 Hz. The strength of the stimulation was adjusted to obtain minimal synaptic responses and was ~20 to 30% above the threshold value (Fig. 1). All evoked responses reported here follow this single-fiber stimulation protocol. Recordings were rejected if the latency of the response changed with stimulation strength or frequency. Pharmacological agents were added to the perfusion medium. All recordings were done at room temperature (20° to 23°C). No outward synaptic currents were recorded at 0-mV holding potential, indicating that $GABA_A$ and $GABA_B$ responses were completely blocked. Responses were filtered (1 kHz) and amplified with an Axopatch 1D, digitized (3 to 10 kHz), and stored on computer for later analysis. In about half the neurons recorded, the pipette solution also included Lucifer yellow, to allow reconstruction of the neuronal morphology at the end of the recording session. A low-magnification brightfield image of the tectum was taken to record the relative position of the cell body within the tectum.
24. M. Rastaad, *Eur. J. Neurosci.* **7**, 1882 (1995). In general (18/20 recordings), the minimal stimulus required to produce a postsynaptic response was the same for depolarized and hyperpolarized holding potentials.
25. C. Allen and C. F. Stevens, *Proc. Natl. Acad. Sci. U.S.A.* **91**, 10380 (1994).
26. G.-Y. Wu, R. Malinow, H. T. Cline, data not shown.
27. AMPA EPSC amplitudes were determined by measuring the amplitude of the response at −60 mV during a 2- to 5-ms window that included the peak response, and subtracting the amplitude of the response immediately before a stimulus. For estimation of the NMDA component, the amplitude of the response during a 10-ms window (~20 ms after the response onset) is measured at +55 mV, and a baseline value obtained immediately before a stimulus is subtracted. At 20 ms after response onset, the AMPA component has decreased so that it contributes <5% of the total current (Fig. 2A).
28. B. Katz, *The Release of Neurotransmitter Substances* (Liverpool Univ. Press, Liverpool, 1969).
29. For recordings of spontaneous mEPSCs, 1 μM tetrodotoxin was added to the bathing solution. mEPSCs were detected with a program as described [N. Otmakhov, A. M. Shirke, R. Malinow, *Neuron* **10**, 1101 (1993)].
30. Amplitude distribution histograms and the rate of failures of synaptic transmission were estimated at hyperpolarized and depolarized potentials by eliciting transmission (50 to 200 trials) at a constant holding potential (−60 or +55 mV), which constitutes an epoch. Depolarizing and hyperpolarizing epochs were interleaved, and data from each holding potential were pooled. The amplitude of individual EPSCs was measured over a 2- to 5-ms window that includes the peak response at −60 mV, and subtracting the amplitude during a window obtained immediately before the stimulus. For a given experiment, the same windows were used to measure responses

at depolarized and hyperpolarized potentials. The smoothed amplitude distribution histograms of responses and noise were generated as described [R. Malinow, *Science* **252**, 722 (1991)]. The peak at zero amplitude represents failures of synaptic transmission and matched the amplitude distribution of the noise (mean ± SD: 0.82 ± 0.07 pA at −60 mV and 0.90 ± 0.09 pA at +55 mV; n = 16). The rate of failures was measured by doubling the fraction of responses with amplitudes less than zero (7). The failure rates at depolarized (F_d) and hyperpolarized (F_h) potentials are approximated by $F_h = (1 - Pr)^{nAN}$ and $F_d = (1 - Pr)^{(nAN + nN)}$, where n_{AN} is the number of releasing sites producing AMPA responses and n_N is the number of releasing sites producing only NMDA responses. *Pr* is the probability of release and is assumed to be similar in both kinds of synapses given that a 15-fold change in probability of release does not appreciably change the AMPA/NMDA ratio [D. J. Perkel and R. A. Nicoll, *J. Physiol.* **471**, 481 (1993)]. (A similar calculation for failure rate is obtained if a heterogeneous, rather than a single, probability of release is assumed.) Rearrangement yields the fraction of pure NMDA responses: $n_N/(n_{AN} + n_N) = 1 - (\ln F_h/\ln F_d)$. The difference in failure rate at −60 mV and at +55mV was eliminated by 100 μM APV (failure rate at hyperpolarized potentials = 0.55 ± 0.08, at depolarized potentials = 0.23 ± 0.07, and at depolarized potentials with APV = 0.54 ± 0.09; n = 4). Pure NMDA responses can be attributed to the existence of synapses with only functional NMDA receptors (7–9). It is unlikely that the absence of AMPA responses at some synapses is due to greater electrotonic filtering of the faster AMPA response, because immature cells are more compact and yet have more, not less, synapses with only NMDA responses (Fig. 4G).

31. G. Carmignoto and S. Vicini, *Science* **258**, 1007 (1992).
32. S. Hestrin, *Nature* **357**, 686 (1992).
33. Vaccinia virus constructs (*20*) were injected into the brain ventricle of stage 44 to 45 tadpoles (*22*). Three days later, when the animal was at stage 47 to 48, the brain was dissected and used for recordings. Animals infected at the same time were stained in wholemount with X-Gal to test for β-Gal expression. Infection of amphibian cells with vaccinia virus does not result in decreased cell density (*14*, *22*), arguing against a cytotoxic action of the virus in this species.
34. D. Liao and R. Malinow, *Learn. Mem.*, in press.
35. K. Fox, H. Sato, N. Daw, *J. Neurosci.* **9**, 2443 (1989).
36. M. C. Crair and R. C. Malenka, *Nature* **375**, 325 (1995).
37. Only two cells had all evoked responses mediated by only NMDA receptors. This paucity can be explained if a single axon makes a number of contacts onto each postsynaptic cell. The gradual change in fraction of pure NMDA responses across the RC axis then reflects addition of AMPA receptor function to individual contacts already showing NMDA receptor function. An alternative interpretation is that pure NMDA responses are due to spillover of transmitter from nearby synapses. In this instance, during development there must be a decrease in spillover (to account for the lower fraction of pure NMDA responses) and a compensating increase in probability of release (to maintain NMDA transmission constant). Furthermore, postsynaptic increase in CaMKII must also decrease spillover and increase probability of transmitter release (to explain similar changes in caudal cells infected with tCaMKII-VV). However, rostral cells infected with tCaMKII-VV showed no change in failure rates (either hyperpolarized or depolarized) (*26*), further arguing against this spillover model. Rostral cells infected with tCaMKII-VV did show an increase in AMPA receptor transmission with little change in NMDA receptor transmission. This result likely reflects the fact that rostral neurons in these animals continued to develop throughout the tadpole stage of development.
38. H. T. Cline, *Trends Neurosci.* **14**, 104 (1991).
39. Sources of the depolarization in the most caudal region of tectum, where the neurons have predominantly NMDA responses, could be intrinsic membrane oscillations or depolarizing GABAergic inputs [E. Cherubini, J. L. Gaiarsa, Y. Ben Ari, *Trends Neurosci.* **14**, 515 (1991)].

40. Supported by the NIH (R.M.), and the National Science Foundation, NIH, and National Down Syndrome Society (H.T.C.). We thank J. Lisman for comments on the manuscript, and members of the labs for helpful discussions.

14 June 1996; accepted 18 September 1996

Distinct Mechanisms for Synchronization and Temporal Patterning of Odor-Encoding Neural Assemblies

Katrina MacLeod and Gilles Laurent*

Stimulus-evoked oscillatory synchronization of neural assemblies and temporal patterns of neuronal activity have been observed in many sensory systems, such as the visual and auditory cortices of mammals or the olfactory system of insects. In the locust olfactory system, single odor puffs cause the immediate formation of odor-specific neural assemblies, defined both by their transient synchronized firing and their progressive transformation over the course of a response. The application of an antagonist of ionotropic γ-aminobutyric acid (GABA) receptors to the first olfactory relay neuropil selectively blocked the fast inhibitory synapse between local and projection neurons. This manipulation abolished the synchronization of the odor-coding neural ensembles but did not affect each neuron's temporal response patterns to odors, even when these patterns contained periods of inhibition. Fast GABA-mediated inhibition, therefore, appears to underlie neuronal synchronization but not response tuning in this olfactory system. The selective desynchronization of stimulus-evoked oscillating neural assemblies in vivo is now possible, enabling direct functional tests of their significance for sensation and perception.

Although stimulus-evoked oscillatory synchronization of neuronal assemblies has been observed in many sensory systems (*1–3*), the mechanisms (cellular, synaptic, and network) underlying coherent recruitment of neurons still remain elusive (*4*). Consequently, it has not yet been possible to selectively alter or suppress the synchronization of such assemblies in vivo, a step essential to test their functional significance for neural coding. The possible functions (if any) of neural synchronization thus remain largely unknown. In the vertebrate olfactory system, bursts of odor-evoked γ (30 to 60 Hz) oscillations ("induced waves") can be seen in the olfactory bulb electroencephalogram during each respiratory cycle (*5*). Induced waves are generated within the bulb (*1*) and have been postulated to result from negative-feedback interactions between granule and mitral cell populations (*6*).

Odor-evoked synchronization of firing has been observed also in the locust *Schistocerca americana* (*7*). In the locust, odors puffed on an antenna cause the synchronization of groups of antennal lobe projection neurons (PNs) (the functional analogs of vertebrate olfactory bulb mitral-tufted cells), resulting in 20- to 30-Hz local field potential (LFP) oscillations in the mushroom body (the functional analog of the piriform cortex) and in subthreshold oscillatory responses in its intrinsic neurons, the Kenyon cells (KCs) (*7*). Although odor puffs evoke long oscillatory LFP bursts, individual PNs generally participate in the synchronized ensembles only for short epochs, but at times that are both neuron- and odor-specific (*7*). The bursts of odor-evoked LFP oscillations therefore result from dynamic neural ensembles whose components (the PNs) phase-lock transiently to one another and change reliably during a single odor response (*2*, *7*). To assess whether the periodic neural synchronization results primarily from local feedback inhibition, as hypothesized for the vertebrate olfactory system (*6*), we studied directly the role of local neurons (LNs) in synchronizing groups of PNs in the antennal lobe of the locust olfactory system.

Intracellular labeling of local neurons (*8*) revealed extensive dendritic arbors throughout the entire antennal lobe neuropil, providing a potential morphological substrate for widespread synchronization (Fig. 1A). Simultaneous intracellular recordings were made from synaptically connected local and projection neurons in vivo (n = 4 pairs) (Fig. 1B). They revealed that, during odor responses, the timing of the periodic depolarization in LNs corresponds precisely to that of the periodic hyperpolarization in postsynaptic PNs, and showed directly that LNs lead PNs by a quar-

California Institute of Technology, Biology Division, 139-74, Pasadena, CA 91125, USA.

*To whom correspondence should be addressed. E-mail: laurentg@starbase1.caltech.edu